Multiscale approach to CO$_2$ hydrate formation in aqueous solution: Phase field theory and molecular dynamics. Nucleation and growth

György Tegze,[a] Tamás Pusztai, Gyula Tóth, and László Gránásy
Research Institute for Solid State Physics and Optics, P.O. Box 49, H-1525 Budapest, Hungary

Atle Svandal, Trygve Buanes, Tatyana Kuznetsova, and Bjørn Kvamme
Institute of Physics and Technology, University of Bergen, Allégaten 55, N-5007 Bergen, Norway

A phase field theory with model parameters evaluated from atomistic simulations/experiments is applied to predict the nucleation and growth rates of solid CO$_2$ hydrate in aqueous solutions under conditions typical to underwater natural gas hydrate reservoirs. It is shown that under practical conditions a homogeneous nucleation of the hydrate phase can be ruled out. The growth rate of CO$_2$ hydrate dendrites has been determined from phase field simulations as a function of composition while using a physical interface thickness (0.85±0.07 nm) evaluated from molecular dynamics simulations. The growth rate extrapolated to realistic supersaturations is about three orders of magnitude larger than the respective experimental observation. A possible origin of the discrepancy is discussed. It is suggested that a kinetic barrier reflecting the difficulties in building the complex crystal structure is the most probable source of the deviations. © *2006 American Institute of Physics.* [DOI: 10.1063/1.2207138]

I. INTRODUCTION

Natural gas hydrates are available in abundance in underwater reservoirs: The amount of carbon bound in natural gas hydrates is conservatively estimated to be twice the amount of carbon to be found in fossil fuels on earth.[1] Under conditions typical for the underwater hydrate reservoirs (temperatures ranging from −1 °C to a few °C and pressures in the range of 5–20 MPa), the natural gas hydrates can be converted to the significantly more stable CO$_2$ hydrate in the presence of liquid CO$_2$ or aqueous CO$_2$ solution while the natural gas is released. This process is considered as a potential candidate for depositing the ever-increasing quantities of industrial CO$_2$, as it may become economic owing to the associated natural gas production. Besides offering a way to reduce the quantity of one of the most important greenhouse gases, this process might also ease/solve the energy problems expected when exhausting the oil reserves. One of the main obstacles of developing appropriate technologies for the exploitation of the natural gas hydrate reserves is the lack of information on the kinetics of the relevant chemical reactions. The kinetics of the CO$_2$ hydrate formation in aqueous solutions is one of the processes of interest. While laboratory experiments indicate that CO$_2$ hydrate dendrites grow at a rate of ν=55 μm/s at 9 K undercooling in a supersaturated aqueous solution,[2] there is a general lack of information on the nucleation and growth rates under other conditions.[3] In a recent paper, we applied the phase field theory to predict the formation of CO$_2$ hydrate.[4,5] The phase field theory is one of the most potent continuum methods that are used to describe solidification phenomena[6–8] including the homogeneous and heterogeneous nucleation[6(d),7] and the growth of complex crystallization morphologies.[6,8] Multiscale approaches based on continuum models that use model parameters obtained from atomistic simulations proved successful in quantitatively predicting nucleation rates[6(d),7(a)–7(d),7(f)] and growth rates of dendritic crystals.[6(c)]

In this paper, such a multiscale approach is used to address the formation of CO$_2$ hydrate in supersaturated aqueous solutions: We perform molecular dynamics simulations with realistic interaction potentials to determine the thickness of the CO$_2$-hydrate–aqueous-solution interface. This interface thickness together with the experimental interfacial free energy is used to fix the model parameters of the phase field theory. Phase field calculations are then performed to determine the rate of the homogeneous nucleation and the velocity of the growth of CO$_2$ hydrate in the dendritic form.

The paper is structured as follows. In Sec. II, we describe the phase field model used in studying hydrate nucleation and growth and the molecular dynamics simulations used to investigate the interface properties. In Sec. III the bulk physical properties of the CO$_2$-hydrate–aqueous-solution system are compiled. In Sec. IV we present our results: First, the equilibrium properties of the aqueous-solution-CO$_2$-hydrate interface are investigated using molecular dynamics simulations. This is followed by presenting the results of phase field calculations for the formation of CO$_2$ hydrate in aqueous solutions. A summary of the results is given in Sec. V.

II. MULTISCALE APPROACH TO GAS HYDRATE FORMATION

Following previous works[6(c),7(c),7(d),7(f)] we apply the phase field approach with model parameters deduced from

---

[a] Author to whom correspondence should be addressed. Fax: +36 1 392 2219; Electronic mail: turpi@szfki.hu

124, 234710-1

atomistic simulations and/or experiments. Within the framework of the phase field theory, we are going to address various phenomena, including nucleation and dendritic growth. The formulation of the theory is described in Sec. II A, while the details of the atomistic simulations for the hydrate-aqueous-solution interface are presented in Sec. II B.

A. Phase field theory

The local state of the matter is characterized by two fields: The nonconserved *phase field* ϕ, which monitors the transition between the liquid and crystalline phases, related to the structural order parameter as $m = 1 - \phi$, and the conserved field,[9] the coarse-grained CO_2 concentration c.

The structural order parameter m can be viewed as the Fourier amplitude of the dominant density wave of the time averaged singlet density in the solid. As pointed out by Shen and Oxtoby,[10] if the density peaks in the solid can be well approximated by Gaussians placed to the atomic sites, all Fourier amplitudes can be expressed uniquely in terms of the amplitude of the dominant wave: thus a single structural order parameter suffices in expanding the free energy. For historic reasons,[11] we take $\phi = 0$ in the solid and $\phi = 1$ in the liquid. Furthermore, we neglect the density difference between the solid and liquid phases, which, together with mass conservation, implies that the integral of the concentration field over the volume of the system is a constant. (Work is underway to incorporate the change of molar volume upon the hydrate formation, an extension of the theory that requires a hydrodynamic approach.)

In the present work, the free energy of the inhomogeneous system is assumed to be a simple local functional of the phase and concentration fields:

$$F = \int d^3r \left\{ \frac{1}{2} \varepsilon^2 T s(\vartheta, \theta)^2 (\nabla \phi)^2 + f(\phi, c) \right\}. \tag{1}$$

This form of the free energy functional is fully consistent with the entropy-functional-based theory by Warren and Boettinger.[11] Here ε is a constant, T is the temperature, and $f(\phi, c)$ is the local free energy density. The gradient term for the phase field leads to a diffuse crystal-liquid interface, a feature observed both in experiment[12] and computer simulations.[13] The local free energy density is assumed to have the form $f(\phi, c) = wTg(\phi) + [1 - p(\phi)]f_S(c, T) + p(\phi)f_L(c, T)$, where the "double well" and "interpolation" functions have the forms $g(\phi) = \frac{1}{4}\phi^2(1 - \phi)^2$ and $p(\phi) = \phi^3(10 - 15\phi + 6\phi^2)$, respectively, that emerge from the thermodynamically consistent formulation of the phase field theory (PFT).[11,14] The respective free energy surface has two minima, whose relative depth, the driving force for crystallization, is a function of both temperature and composition as specified by the free energy densities in the bulk solid and liquid, $f_{S,L}(c, T)$. The free energy scale w determines the height of the free energy barrier between the bulk solid and liquid states.

The dependence of the surface energy on the orientation of the liquid-solid interface is introduced through the function $s(\vartheta, \theta) = 1 + s_0 \cos[k(\vartheta - 2\pi\theta/k)]$, which multiplies the penalty for gradients in ϕ.[15] Here s_0 is the "anisotropy" pa-

rameter, and k is the symmetry index (e.g., $k = 4$ stands for the fourfold symmetry of the interfacial free energy), $\vartheta = \arctan[(\nabla \phi)_y/(\nabla \phi)_x]$ is the inclination of the solid-liquid interface in the laboratory frame, and $\theta \in [0, 1]$ is the normalized inclination angle determining the crystal orientation in the laboratory frame.

Provided that the bulk thermodynamic properties $f_L(c, T)$ and $f_S(c, T)$ are known, the only model parameters remaining undetermined are ε and w, which we assume independent of composition, for the sake of simplicity. These model parameters can be related to measurable quantities characterizing the equilibrium planar interface (see Sec. II A 1) emerging between the coexisting solid and liquid phases (of compositions determined by the common tangent construction).

Once the free energy functional is specified, the height of the nucleation barrier and the equations of motion that describe the time evolution of the system can be obtained following the practice of the classical field theory.

1. Equilibrium interface

The CO_2 hydrate and the aqueous solution of CO_2 of appropriate compositions (c_S^e and c_L^e, respectively) coexist under conditions typical to medium depths. The phase and concentration field profiles that are realized under such conditions minimize the free energy of the *planar interface*. This extremum of the free energy functional is subject to the solute conservation constraint discussed above. To impose this constraint one adds the volume integral over the conserved field times a Lagrange multiplier λ to the free energy: $\lambda \int d^3r\, c(\mathbf{r})$. The field distributions that extremize the free energy obey the appropriate Euler-Lagrange (EL) equations[16]

$$\frac{\delta F}{\delta \phi} = \frac{\partial I}{\partial \phi} - \nabla \frac{\partial I}{\partial \nabla \phi} = 0 \tag{2a}$$

and

$$\frac{\delta F}{\delta c} = \frac{\partial I}{\partial c} - \nabla \frac{\partial I}{\partial \nabla c} = 0, \tag{2b}$$

where $\delta F/\delta \phi$ and $\delta F/\delta c$ stand for the first functional derivative of the free energy with respect to the fields ϕ and c, respectively, while $I = \frac{1}{2}\varepsilon^2 T(\nabla \phi)^2 + f + \lambda c$ is the total free energy density inclusive of the term with the Lagrange multiplier. The EL equations have to be solved under the boundary conditions that bulk hydrate and liquid solution phases of the equilibrium compositions exist at $z \to \pm\infty$, respectively. Under such conditions, the Lagrange multiplier can be identified as $\lambda = -(\partial I/\partial c)_{z \to \pm\infty} = -(\partial f_S/\partial c)(c_S^e) = -(\partial f_L/\partial c)(c_L^e)$.

Considering these and an isotropic interface ($s_0 = 0$), the EL equations can be rewritten as[6]

$$\frac{\varepsilon^2 T}{2} \left(\frac{d\phi}{dz} \right)^2 = \Delta f(\phi, c) \tag{3a}$$

and

$$0 = wTg(\phi) + [1 - p(\phi)]\frac{\partial f_S}{\partial c} + p(\phi)\frac{\partial f_L}{\partial c} - \frac{\partial f_L}{\partial c}(c_L^e), \tag{3b}$$

where $\Delta f = f - f_{\pm\infty} - \lambda(c - c_{\pm\infty})$ and subscripts $\pm\infty$ indicate values at $+\infty$ and $-\infty$, respectively. Note that $f_{\pm\infty} + \lambda(c - c_{\pm\infty})$

$=f_L(c_L^e)+(\partial f_L/\partial c)(c_L^e)[c-c_L^e]=f_S(c_S^e)+(\partial f_S/\partial c)(c_S^e)[c-c_S^e]$ is the equation of the common tangent. Since the right hand side of Eq. (3b) is a function of the fields c and ϕ, it provides the implicit relationship $c=c(\phi)$ [which can be determined by inverting Eq. (3b) numerically]. The phase field profile is then obtained by expressing $dz/d\phi$ from Eq. (3a) and integrating it with respect to ϕ after inserting $c=c(\phi)$:

$$z-z_0=\left(\frac{\varepsilon^2 T}{2}\right)^{1/2}\int_{\phi_0}^{\phi}d\xi\{\Delta f[\xi,c(\xi)]\}^{-1/2}. \qquad (4)$$

Then, the 10%–90% thickness of the interface reads as

$$d=\left(\frac{\varepsilon^2 T}{2}\right)^{1/2}\int_{0.1}^{0.9}d\xi\{\Delta f[\xi,c(\xi)]\}^{-1/2}. \qquad (5)$$

After trivial manipulations of Eq. (3a),[16] the free energy of the solid-liquid interface can be expressed as

$$\gamma_{\infty}=(2\varepsilon^2 T)^{1/2}\int_{0}^{1}d\xi\{\Delta f[\xi,c(\xi)]\}^{1/2}. \qquad (6)$$

The two-dimensional Newton-Raphson iteration based on Eqs. (5) and (6) has been used to find those values of the model parameters ε and w by which the known values of d and γ_{∞} are recovered.

2. Calculation of the nucleation barrier

The crystallization of nonequilibrium liquids starts with nucleation, a process in which crystal-like fluctuations appear, whose formation is governed by the free energy gain when transferring molecules from liquid to the crystal and the extra free energy γ needed to create the crystal-liquid interface.[17–19] The fluctuations larger than a critical size have a good chance to reach macroscopic dimensions, while the smaller ones dissolve with a high probability. Being in an unstable equilibrium, the critical fluctuation (the nucleus) can be found as an extremum (saddle point) of this free energy functional,[7,18,19] subject again to the solute conservation discussed above. The field distributions that extremize the free energy obey again the respective EL equations, Eqs. (2a) and (2b).[18] These EL equations are to be solved, assuming that unperturbed liquid ($\phi=0$, $c=c_{\infty}$) exists in the far field, while for symmetry reasons zero field gradients appear at the center of the fluctuations. Under such conditions, the Lagrange multiplier can be identified as $\lambda=-(\partial I/\partial c)_{r\to\infty}=-(\partial f_L/\partial c)(c_{\infty})$.

Assuming a spherical symmetry ($s_0=0$), which is reasonable considering the low anisotropy of the crystal-liquid interface of simple liquids at small undercoolings, the EL equations can be rewritten as

$$\varepsilon^2 T\left\{\frac{d^2\phi}{dr^2}+\frac{2}{r}\frac{d\phi}{dr}\right\}=wTg'(\phi)+p'(\phi)\{f_L(c)-f_S(c)\}$$

$$(7a)$$

and

$$0=wTg(\phi)+[1-p(\phi)]\frac{\partial f_S}{\partial c}+p(\phi)\frac{\partial f_L}{\partial c}-\frac{\partial f_L}{\partial c}(c_{\infty}). \qquad (7b)$$

Here the prime (′) stands for differentiation with respect to the argument of the function. Again, the EL equation for the concentration field defines the implicit relationship $c=c(\phi)$ [which has been obtained by inverting Eq. (7b) numerically]. Accordingly, Eq. (7a) is an ordinary differential equation for $\phi(r)$. This equation has been solved here numerically using a fourth order Runge-Kutta method. Since ϕ and $d\phi/dr$ are fixed at different locations, the central value of ϕ that satisfies $\phi\to\phi_{\infty}=1$ for $r\to\infty$ has been determined interactively. Having determined the solutions $\phi(r)$ and $c(r)$, the work of the formation of the nucleus W^* has been obtained by inserting these solutions into the free energy functional. Provided that the model parameters w and ε have been evaluated from the thickness and free energy of the equilibrium planar interface, the work of the formation of the critical fluctuation W^* in the supersaturated state can be calculated *without adjustable parameters*.

The steady state nucleation rate (the net number of critical fluctuations formed in unit volume and time), J_{SS}, can be computed as

$$J_{SS}=J_0\exp\{-W^*/kT\}, \qquad (8)$$

using the classical nucleation prefactor.[20] J_0 verified experimentally on oxide glasses.[21]

3. Phase field simulation of single crystal growth

Time evolution is assumed to follow relaxational dynamics[6]

$$\dot{\phi}=-M_{\phi}\frac{\delta F}{\delta\phi}=M_{\phi}\left\{\nabla\left(\frac{\partial I}{\partial\nabla\phi}\right)-\frac{\partial I}{\partial\phi}\right\} \qquad (9a)$$

and

$$\dot{c}=\nabla M_c\nabla\frac{\delta F}{\delta c}=\nabla\left\{M_c\nabla\left[\left(\frac{\partial I}{\partial c}\right)-\nabla\left(\frac{\partial I}{\partial\nabla c}\right)\right]\right\}. \qquad (9b)$$

The time scales for the two fields are determined by the appropriate mobilities appearing in the equations of motion, and M_{ϕ} and M_c are the mobilities associated with the coarse-grained equation of motion, which in turn are related to their microscopic counterparts. The mobility M_c is directly proportional to the classic interdiffusion coefficient for a binary mixture, while the mobility M_{ϕ} dictates the rate of crystallization. A recent experiment has shown that the rate of crystallization in highly supercooled liquids is proportional to the translational diffusion coefficient (D_{tr}),[22] which is, in turn, related to the viscosity (η) as $D_{tr}\propto\eta^{-0.74}$. In our model, the growth velocity scales linearly with M_{ϕ}, so consistency requires $M_{\phi}\propto D_{tr}$.

(1) *Equations of motion-phase field*: Using the length and time scales ξ and ξ^2/D_l, respectively, where D_l is the chemical diffusion coefficient in the liquid, the dimensionless phase field mobility $m_{\phi}=M_{\phi}\alpha_0^2 T/D_l$, the following *dimensionless form* emerges,

$$\widetilde{\dot{\phi}} = m_\phi \Bigg[\widetilde{\nabla}(s^2 \widetilde{\nabla} \phi) - \frac{\partial}{\partial \widetilde{x}} \left\{ s \frac{\partial s}{\partial \vartheta} \frac{\partial \phi}{\partial \widetilde{y}} \right\} + \frac{\partial}{\partial \widetilde{y}} \left\{ s \frac{\partial s}{\partial \vartheta} \frac{\partial \phi}{\partial \widetilde{x}} \right\}$$
$$- \xi^2 \frac{w(c) T g'(\phi) + p'(\phi)\{f_L(c,T) - f_S(c,T) - f_{\text{cri}}\}}{\varepsilon_\phi^2 T} \Bigg].$$

$$(10)$$

(Henceforth, quantities with tilde are dimensionless.)

(2) *Equations of motion-concentration field*: In previous works,[11,23] we choose the mobility of the concentration field as $M_c = (\nu_m / \mathrm{RT}) D c (1-c)$, where ν_m is the average molar volume and $D = D_s + (D_l - D_s)\, p(\phi)$ is the diffusion coefficient. This choice ensures a diffusive equation of motion. Introducing the reduced diffusion coefficient $\lambda = D/D_l$, the *dimensionless equation of motion* for the concentration field reads as

$$\widetilde{\dot{c}} = \widetilde{\nabla} \Bigg\{ \frac{\nu_m}{\mathrm{RT}} \lambda c (1-c) \widetilde{\nabla} \Bigg[(w_B - w_A) T g(\phi)$$
$$+ [1 - p(\phi)] \frac{\partial f_S}{\partial c}(c,T) + p(\phi) \frac{\partial f_L}{\partial c}(c,T) \Bigg] \Bigg\}.$$

$$(11)$$

The time evolution of the system is studied by solving Eqs. (10) and (11) numerically in two dimensions (2D). Details of the numerical solution are reviewed in Sec. II A 4.

It is appropriate to call attention to the limitations of the phase field approach. The main difficulty *quantitative* phase field modeling has to face is that a subnanometer spatial resolution is needed in the interfacial region that extends to a couple of nanometers according to experiment[12] and computer simulations.[13] This diffuseness of the interface is recovered in the phase field models as a result of the square-gradient terms in the free energy, which penalize sharp changes of the fields. The interface thickness is usually orders of magnitude smaller than the objects of interest; thus the numerical solution of the equations, at the resolution required to describe the nanometer thick diffuse interfaces properly, is, in general, limited to small systems (in two and higher dimensions). To overcome this difficulty, different methods have been worked out.

(i)   To ensure the proper interface dynamics, the model parameters are adjusted and interface currents (i.e., a new term in the phase field equations) are introduced to compensate for the unphysical effects of the broad interface.[24] These methods make a *quantitative* phase field modeling of dendritic solidification feasible for thermal dendrites and dendrites in dilute solutions.[24(b),25] While quantitative simulations of such dendrites with model parameters fixed by atomistic simulations is perhaps the most spectacular successes of theory, a generally applicable approach (that could be used for the hydrate formation) has yet to be developed.

(ii) The application of an adaptive grid that is fine at the interfaces can reduce the numerical problems tremendously.[26] However, noise needs to be introduced into the governing equations to obtain realistic morphologies,[11] and this is expected to lead to nontrivial problems in the case of models of unequal cell sizes that need to be clarified first.

Thus, techniques (i) and (ii) cannot be easily adapted to the hydrate formation, as the aqueous-solution–CO_2-hydrate system is far from being a dilute solution, and as we wish to take into account the effect of noise in obtaining the growth morphology. Therefore, in the present paper, we perform quantitative simulations with the physical interface thickness relying on efficient algorithms (a spectral method) and parallel computing. This evidently limits the size and time available for the simulations. We, therefore, investigate the sensitivity of the results to the broadening of the interfaces to see whether it is possible to make simulations that are less costly but still reasonably accurate.

A further difficulty associated with quantitative phase field calculations is that the detailed information on the system needed for such computations, such as the magnitude and anisotropy of the phase field mobility and the interfacial free energy, are generally inaccessible. Linking the phase field theory with atomistic simulations via evaluating the model parameters (mobility, anisotropies, and interfacial free energy) from the molecular dynamics simulation is a possible resolution to this problem.[6(c),27]

4. Numerical implementation

The governing equations have been solved numerically using a semi-implicit spectral scheme. To generate sufficiently smooth initial conditions, the first time steps were done by explicit finite difference (FD) discretization. The computational cost of a single implicit step is about five times larger than that of an explicit FD step; however, the length of the implicit time step can be about 150–300 times longer than the explicit step. We have prescribed periodic boundary conditions. In a few cases, the same problem has been solved by both explicit and implicit schemes. A parallel C code has been developed including fast Fourier transform (FFT) that relies on the message passing interface (MPI) protocol. To optimize the performance, we have developed a parallel FFT code based on the FFTW library.[28] Our computations were performed on a PC cluster built up exclusively for phase field calculations at the Research Institute for Solid State Physics and Optics, Budapest. This cluster consists of 100 nodes and a server machine (all equipped with AMD 64 bit processors and 1 Gbit/s communication). Exploratory calculations have also been performed on another computer cluster at the University of Bergen. The present paper is based on computations exceeding 20 CPU years on a 2 GHz processor.

B. Molecular dynamics

Molecular dynamics (MD) simulations were performed to study the microscopic properties of the hydrate–aqueous-fluid interface. The hydrate part of our system comprised a block of structure 1 carbon dioxide hydrate[29,30] made of $2 \times 2 \times 11$ unit hydrate cells [2024 extended single point charge (SPC/E) water[31]] and 264 three-site CO_2 molecules.[32]

The hydrate structure was generated as a perfect equilibrated periodic hydrate crystal arbitrary broken in two and brought into contact with a preequilibrated 40 Å long slab of 795 SPC/E water molecules. The resulting interfacial system ranged about 170 Å in length. Periodic boundary conditions were applied in all three directions.

Our MD routine used the MDYNAMIX package of Lyubartsev and Laaksonen[33] with an explicit reversible integrator for *NPT* dynamics of Martyna *et al.*,[34] modified to implement an implicit quaternion treatment of rigid molecules with Nosé-Hoover thermostat for temperature and pressure.[35–37] The time step was set to 1 fs, with the simulation run totaling upward of 5×10^6 steps. Electrostatic interactions were handled by means of the Ewald summation technique with a variable number of reciprocal vectors. Linux-based MPI was used to implement a parallel computation on a cluster of dual-processor machines.

The system was kept at a constant temperature of 240 K and pressure of 20 MPa by means of Nosé-Hoover thermo- and barostat, where only the tangential components of the pressure tensor were used to evaluate and control the pressure. Bryk and Haymet[38] have shown that the stable ice-water interface of the SPC/E water is located around 225 ± 10 K. Thus the chosen value of 240 K ensures the liquidity of the model water and, at the same time, roughly corresponds to the temperature range used in the phase field simulations.

III. PHYSICAL PROPERTIES

The molar Gibbs free energy of the aqueous CO_2 solution has been calculated as $F_L = (1-c)F_{L,W} + cF_{L,CO_2}$, where c is the mole fraction of CO_2. The partial molar free energy of water in solution has been obtained as $F_{L,W} = F_{L,W}^0 + RT \ln[(1-c)\gamma_{L,W}(c)]$, where the free energy of pure water has been calculated as

$$F_{LW}^0 = \sum_{i=0}^3 \frac{k_i}{T^i}, \qquad (12)$$

with coefficients k_i taken from Ref. 39. Here R is the gas constant and $\gamma_{L,W}$ is the activity coefficient of water in solution. The partial molar free energy of CO_2 in solution is $F_{L,CO_2} = F_{L,CO_2}^\infty + RT \ln[c\ \gamma_{L,CO_2}(c)]$, where the molar free energy of CO_2 at an infinite dilution F_{L,CO_2}^∞ has been fitted to a simple function in temperature from solubility data extracted from the empirical model by Diamond and Akinfiev,[40] at low pressures, where the solubility is very low. The value decreases slightly with temperature and at 274.3 K $F_{L,CO_2}^\infty = -21.50$ J/mol. The activity coefficient of CO_2 in the aqueous solution $\gamma_{L,CO_2}(c)$ has been fitted to solubility data at higher pressures and mole fractions.

$$\ln \gamma_{L,CO_2} = a_1 c + a_2 c^2, \qquad (13)$$

with $a_1 = -2.522 \times 10^3$ and $a_2 = 1.020 \times 10^6$. The activity coefficient of water $\gamma_{L,W}$ in the aqueous solution has been obtained from Eq. (13) via the Gibbs-Duhem relationship.

The free energy of the hydrate is given by $f_S = (1-c)F_{S,W} + cF_{S,CO_2}$. Owing to the lack of experimental information, the partial molar quantities have been calculated using the model described in Ref. 39. For water and CO_2 we use the relationships $F_{S,W} = F_{S,W}^0 + RT(3/23)\ln(1-\theta)$, and $F_{S,CO_2} = F_{S,CO}^{inc} + RT \ln[\theta/(1-\theta)]$, respectively, where the hole occupancy is $\theta = [c/(1-c)]/(3/23)$. Here, the partial molar free energies of the empty clathrate, $F_{S,W}^0$, and that of the guest inclusion, $F_{S,CO}^{inc}$, are given by Eq. (13), with the appropriate k_l taken from Ref. 39. The respective phase diagram and bulk free energies and the free energy surface are shown in Fig. 1. For further details see Ref. 41.

Unless stated otherwise, the computations are performed under conditions typical for the seabed reservoirs, i.e., $T = 274.3$ K, $p = 6.2$ MPa ($\sim$620 m depth); furthermore, we assume that water has been saturated by CO_2 ($c = 0.033$, obtained by extrapolating the relevant data by Teng and Yamasaki[42]). These experimental data are for the synthetic average seawater. The salinity of groundwater in reservoirs may vary from close to zero up to seawater salinity in regions where the penetration of seawater dominates the salinity.

The saturation composition of the aqueous solution as a function of temperature and pressure has been calculated by the computer code of Diamond and Akinfiev.[40] The average molar volume is assumed to be $\nu_m = 18.02$ cm^3/mol. The interfacial properties (interfacial free energy and interface thickness) needed to fix ε and w are taken from experiment and atomistic simulations. The experimental value of the free energy of the CO_2-hydrate-aqueous-solution interface is $\gamma_\infty = 30 \pm 3$ mJ/m^2, evaluated from hydrate dissociation data in mesoporous silica.[43] This magnitude of γ falls close to that of the ice-water interface ($\gamma_\infty = 29.1 \pm 0.8$ mJ/m^2),[44] as expected.[3,45] Unfortunately, the error of the experimental value is quite substantial ($\sim$10%), preventing an accurate calculation of the nucleation rate.

We are unaware of experimental data for the anisotropies of the interfacial free energy. On the basis of the experimental images,[2] we assume a fourfold symmetry ($k=4$) of the interfacial free energy. It appears that under specific conditions the CO_2 dendrites have a faceted morphology that indicates a substantial anisotropy.[46] Considering these, unless stated otherwise the calculations were performed with an anisotropy $s_0 = 0.065$ slightly below the critical one $s_0 = 1/15$, above which excluded directions appear in the equilibrium shape.[47]

Owing to a lack of experimental information on the microscopic properties of the CO_2 hydrate/aqueous solution interface, we used molecular dynamics simulations to evaluate the interfacial density profiles. The envelope of the interfacial density peaks, which may be loosely identified as the spatial variation of the amplitude of the dominant density wave, is fitted with the function

$$X(z) = A + \tfrac{1}{2}B\{1 + \tanh[(z - z_0)/(2^{3/2}\delta)]\}, \qquad (14)$$

where the interface thickness δ is related to the 10%-90% interface thickness d (the distance on which the phase field changes between 0.1 and 0.9) as $d = 2^{5/2} \text{arctanh}(0.8)\ \delta$. Note that this interface profile is strictly valid if the phase field decouples from the concentration field (i.e., chemical effects at the interface are negligible). In practice Eq. (14) seems to approximate the interfacial profiles reasonably well. As de-
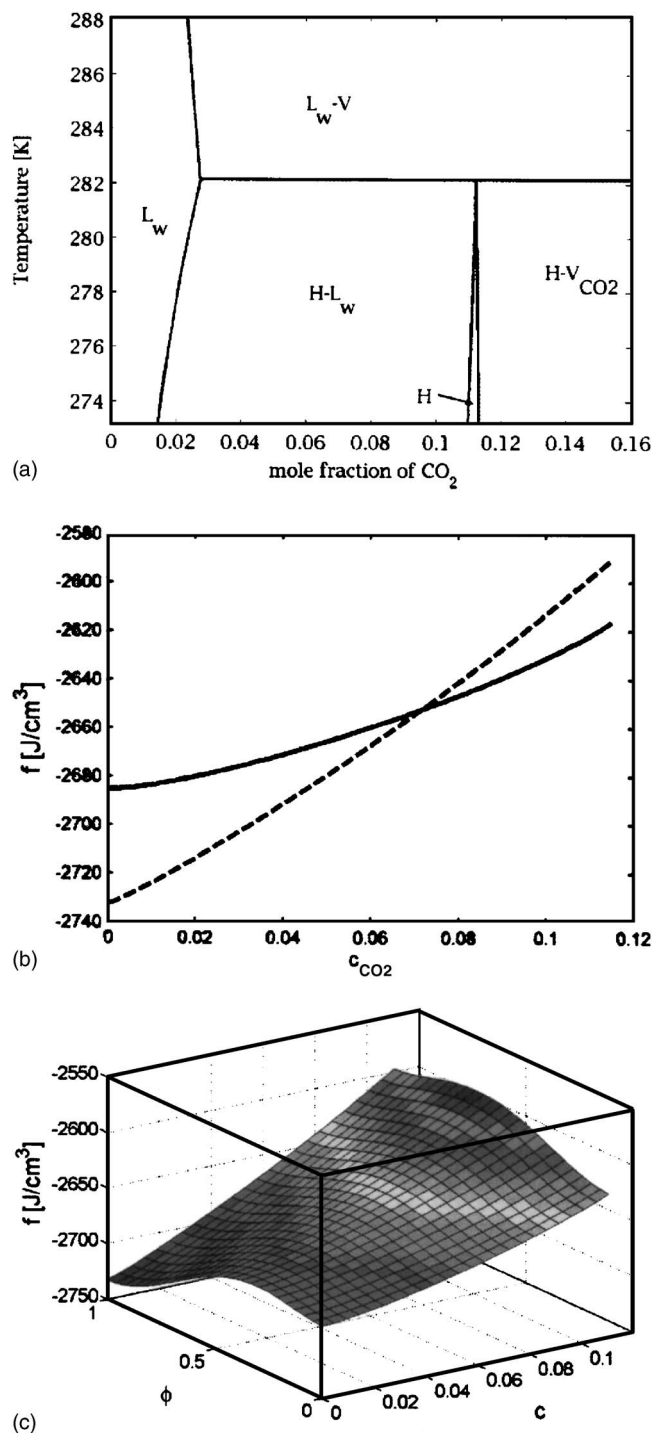
FIG. 1. (a) Calculated isobaric phase diagram of the water-CO_2 system at $p=6.2$ MPa (for details see Ref. 41). Here L_w, H, V, and V_{CO_2} stand for the aqueous solution, the solid hydrate and the vapor phases, respectively. (b) The bulk free energy density as a function of the CO_2 concentration at T $=274.3$ K and $p=6.2$ MPa for the CO_2 hydrate (solid line) and the aqueous solution (dashed line), as specified by Eqs. (13) and (14). (c) The free energy surface $f(\phi,c)$ for the CO_2-hydrate-aqueous-solution system calculated with $w=5.46$ J/(K cm^3) under the same temperature and pressure as panel (b).

tailed in Sec. IV A, d shows some scattering when evaluated from the density or charge density profiles for the two constituents (CO_2 or H_2O). The average value is d $=0.85\pm0.07$ nm. Unless stated otherwise, this value has been used to calculate the model parameters of the phase field theory.

The respective magnitudes of the free energy parameters are $\varepsilon^2=1.25\times10^{-15}$ J/(K cm) and $w=5.46$ J/(K cm^3). The corresponding free energy surface is displayed in Fig. 1(c). In the calculations with the physical interface thickness, the characteristic length scale was chosen as $\xi=10^{-8}$ cm. Unless stated otherwise, for the explicit calculations, the time and spatial steps were $\Delta t=0.04\tau$ and $\Delta x=\xi$, respectively, where $\tau=\xi^2/D_l=5\times10^{-13}$ s. In the case of implicit calculations, the time step was 150 to 300 times larger.

Finally, we need to set the values for the mobilities that fix the time scale for the evolution of the phase and concentration fields. The diffusion coefficient of CO_2 in liquid is $D_l=2\times10^{-4}$ cm^2/s,[48] while the diffusion coefficient in the solid has been assumed to be $D_s=10^{-3}D_1$.

The dimensionless phase field mobility is related to the kinetic coefficient β as $m_\phi=\beta\gamma_\infty Tv_m/(D_l\Delta H_f)$, where ΔH_f is the molar heat of fusion.[11,23] Utilizing that (a) in the Wilson-Frenkel model, applicable to most molecular liquids, β $=D_l\Delta G/(l_0 RT)$, where $l_0\approx\rho^{1/3}$ is the molecular jump distance and $\Delta G>0$ is the molar Gibbs free energy difference between the liquid and the solid, that (b) according to Turnbull's linear approximation $\Delta G\approx\Delta H_f(T_f-T)/T_f$,[49] and that (c) the interfacial free energy can be related to the melting properties as $\gamma_\infty=\alpha\Delta H_f/(N_0^{1/3}v_m^{2/3})$, one finds that m_ϕ $\approx\alpha(\Delta S_f/R)$, where ΔS_f is the entropy of fusion and α is Turnbull's coefficient that is ~0.45 for closed structures and ~0.33 for open structures.[49] Approximating the relevant properties with those of the ice-water system, one finds m_ϕ ≈0.77.

IV. RESULTS AND DISCUSSION

A. The planar hydrate-solution interface

1. Molecular dynamics

The interfacial density and charge density distributions emerging from our molecular dynamics simulations after 19 ps time are shown in Fig. 2. The respective 10%-90% interface widths d evaluated by fitting Eq. (14) to the upper and lower envelopes of the peaks and wells of the layerwise averaged density are presented in Table I. Despite the scattering of the data, the mass and charge density profiles show comparable interface widths, and their average is d_{phys} $=0.85\pm0.07$ nm. (Note that the interface thickness, in which the properties change perceptibly, is about twice of this width, i.e., $d_{full}\approx1.7$ nm, which is still somewhat narrower than reported for other hydrate-liquid interfaces.)

2. Phase field theory

The phase field and concentration profiles calculated using Eqs. (4) and (3b), respectively, are shown in Fig. 3. The phase field profile is very close to the form for the analytical solution for the one-component phase field theory relying on a quartic free energy. A remarkable feature is the rather sharp concentration profile. This requires a spatial step size as low as $\Delta x=0.1$ nm or less in the 2D simulations to resolve the concentration profile with a reasonable accuracy.
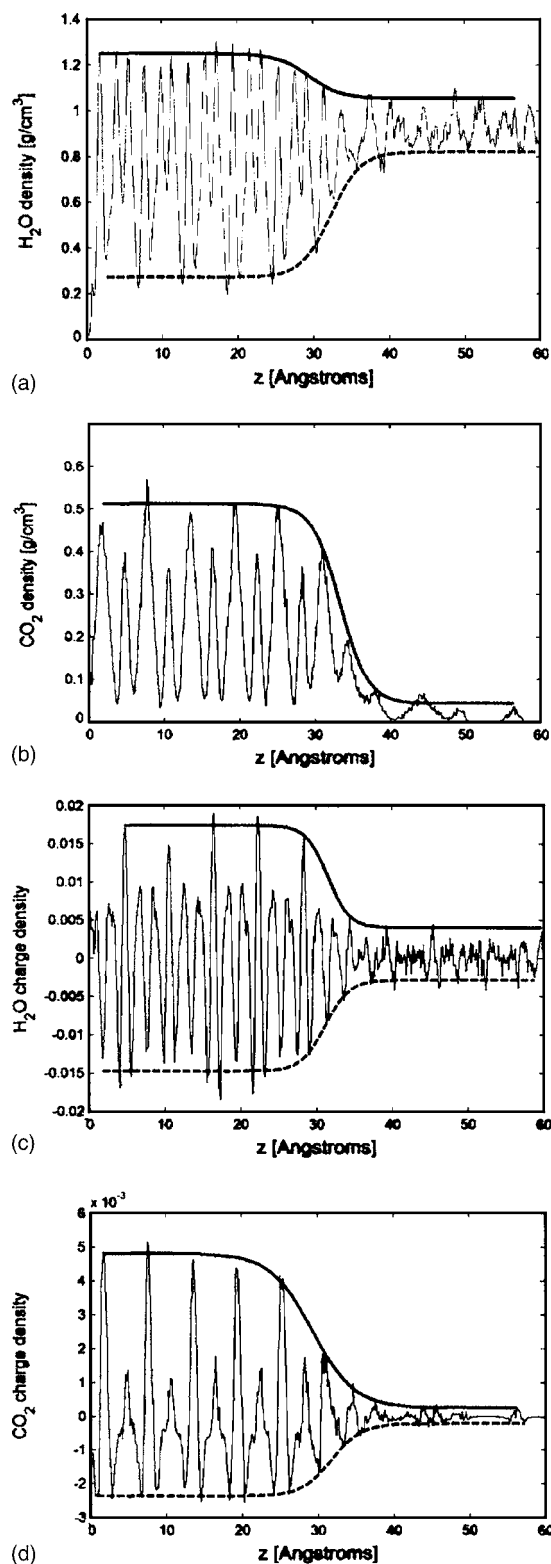
FIG. 2. Interfacial density and charge density profiles and the curves obtained by fitting Eq. (20) to the upper and lower density envelopes. (a) H$_2$O density, (b) CO$_2$ density, (c) H$_2$O charge density, and (d) CO$_2$ charge density.

B. Nucleation of CO$_2$ hydrate

Properties of the critical fluctuations are shown as a function of fluid composition in Fig. 4. As shown by the structural order parameter profiles $[m(r)=1-\phi(r)]$, in the vicinity of the saturation composition for $T=274.3$ K at

TABLE I. 10%–90% interface widths from MD simulations. Notation: D—mass density, CD—charge density, ↑—envelope of peaks, ↓—envelope of wells, and GF—Gaussian filtered.

	d (nm)	σ_d (nm)
H$_2$O D↑	0.93	0.50
H$_2$O D↓	0.86	0.25
CO$_2$ D↑	0.79	0.25
H$_2$O CD↑	0.61	0.30
H$_2$O CD↓	0.69	0.24
CO$_2$ CD↑	1.21	0.19
CO$_2$ CD↓	0.88	0.14
Average	0.85	0.07
H$_2$O DGF	1.21	0.18
CO$_2$ DGF	1.07	0.13

6.2 MPa, the critical fluctuation is far larger than the interface thickness [see Fig. 4(a)]. This suggests that the classical droplet model of the CNT might be a fair approximation [Fig. 4(b)], as reflected by a relatively small difference in the nucleation barrier heights, especially at low supersaturations. However, the exponential term in Eq. (8) converts this difference into a ∼20–50 orders of magnitude difference in the nucleation rates predicted by the two models [Fig. 4(c)]. Whichever model is used, however, in this range the nucleation rate is so small that the appearance of a homogeneous nucleation can safely be excluded. This situation does not change much if the considerable uncertainty of the interfacial free energy is taken into account [Figs. 4(b) and 4(c)] or the temperature/pressure are changed in the ranges 5.0–50.0 MPa corresponding to depths of ∼500–5000 m, or between −1 and 9 °C, respectively [see Figs. 5 and 6].

The present analysis indicates that since the nuclei are quite large with respect to the interface thickness, the CNT predictions for the barrier height fall relatively close to those by the PFT. We arrived at a different conclusion in recent studies[4,5] as a result of the higher driving force used there. Our present analysis indicates that the nucleation rate in the practically interesting domain is far too low to observe a
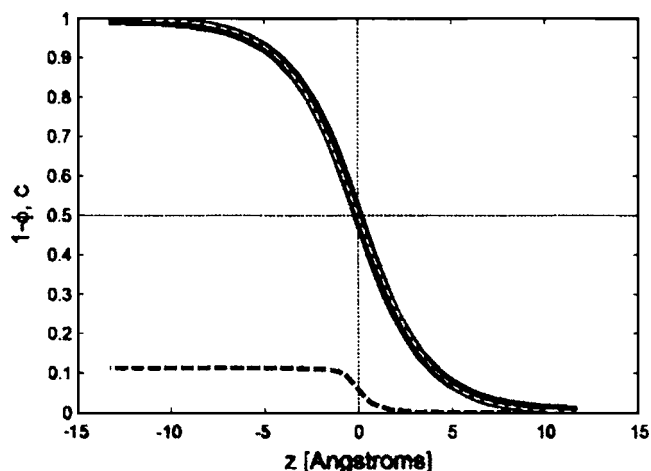

FIG. 3. Interfacial structural order parameter $(1-\phi)$ (heavy solid line) and concentration profiles (dashed line). For comparison the $(1/2)\{1-\tanh[z/(2^{3/2}\delta)]\}$ curve is also shown (white dashed line). Note that the structural order parameter profile is very close to the latter form.
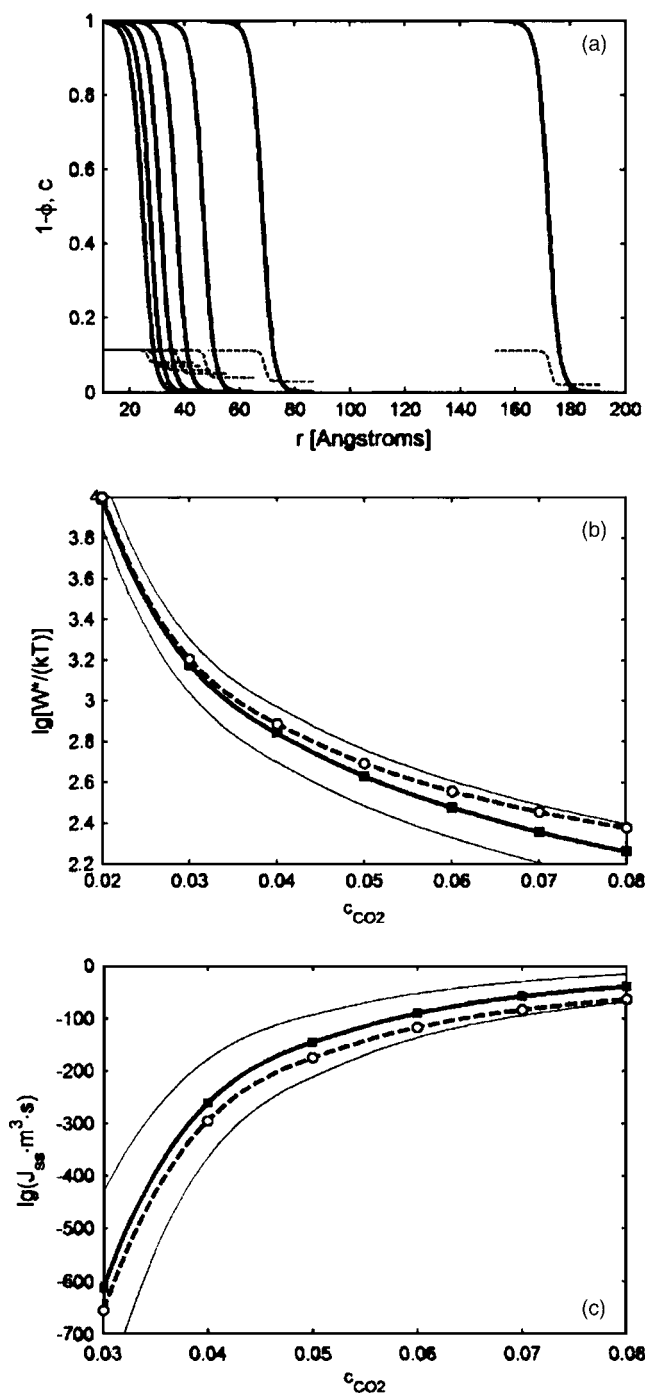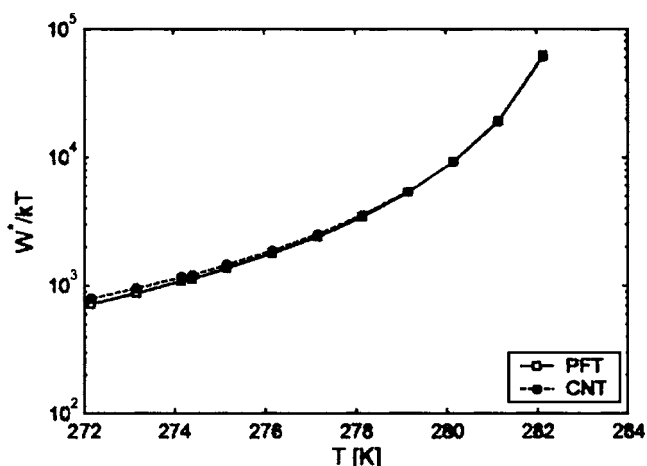
FIG. 5. Height of the nucleation barrier vs temperature as predicted for the saturated aqueous solution at $p=6.2$ MPa by the phase field theory (PFT) and by the droplet approximation of the classical nucleation theory (CNT). Note that due to the large size of the critical fluctuations the classical and nonclassical predictions fall quite close.

Our calculations also indicate that for an accurate prediction of the nucleation rate, the solid-liquid interface free energy has to be determined with a far higher accuracy. Such accuracy can only be expected from molecular dynamics simulations.[27] Work is underway to evaluate this quantity from the interfacial fluctuations.[27(b),27(e)–27(g)]

Finally, it is worth noting that in aqueous CO_2 solutions of viscosity in the mPa s range, the induction time of the hydrate nucleation, after which the steady state cluster distribution is established, is negligible with respect to the time needed to create the first nucleus via a steady state nucleation.[51] Thus transient nucleation effects can safely be neglected. (This is indeed expected in liquids of low viscosity, when the driving force is small enough to yield large-size critical fluctuations that form with a very low probability.)

C. Growth of CO_2 hydrate dendrites in aqueous solution

Since with the present numerical approach the computations with the physical interface thickness are prohibitively

FIG. 4. Properties of critical fluctuations as predicted by the phase field theory. (a) Radial structural order parameter $(1-\phi)$ (heavy solid line) and concentration profiles (dashed line) calculated at $T=274.3$ K and $p=6.2$ MPa, while the mole fraction of CO_2 in the initial fluid phase from left to right was $c=0.08, 0.07, 0.06, 0.05, 0.04, 0.03$, and 0.02. (b) The height of the nucleation barrier as a function of the composition of the aqueous solution. (c) Steady state nucleation rate. In panels (b) and (c) the results from the phase field theory (heavy solid lines) and those from the classical nucleation theory (dashed lines) are compared. The uncertainty of the PFT prediction due to the experimental error of the interface free energy is also shown (thin solid lines). The CNT prediction has a comparable uncertainty.

homogeneous nucleation in this system. This result agrees with the experimental observation that the volume nucleation of CO_2 hydrate is indeed rarely observed in aqueous solutions, and suggests that, when it is seen, it is probably of heterogeneous origin.
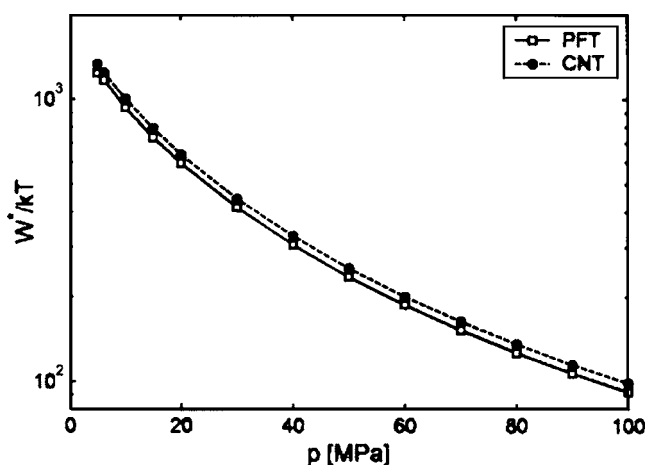

FIG. 6. Height of the nucleation barrier vs pressure as predicted for the saturated aqueous solution at $T=274.3$ K by the phase field theory (PFT) and by the droplet approximation of the classical nucleation theory (CNT).
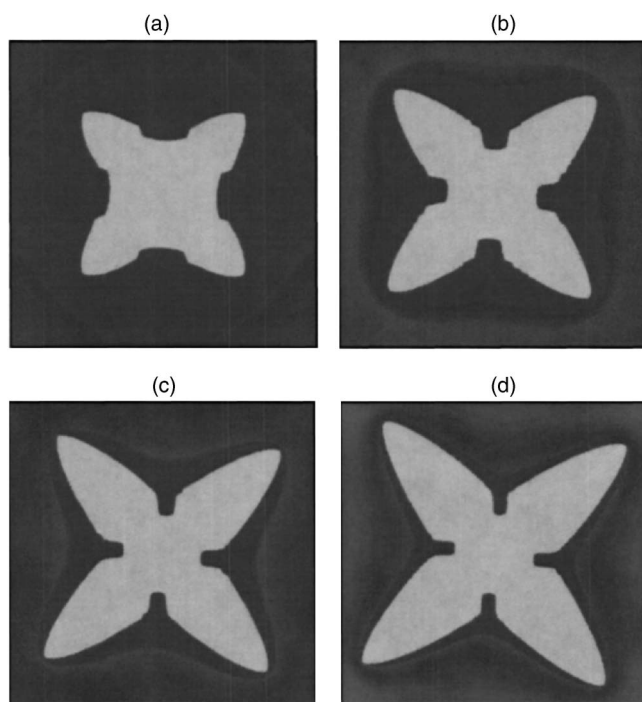
FIG. 7. CO$_2$ hydrate dendrites predicted on a 4096$\times$4096 grid (0.409 $\times$0.409 μm^2) using the *physical interface thickness* in aqueous solutions of CO$_2$ concentrations of (a) $c=0.05$, (b) 0.06, (c) 0.07, and (d) 0.08. Snapshots of the concentration field show states reached after 333, 198, 107, and 63 ns physical time, respectively. Note the dependence of the growth morphology and the growth velocity on the driving force and the variation of the diffusion field around the dendrites.

TABLE II. Infinite time extrapolation of growth velocity v. Notation: d_{phys}—physical interface thickness; d—interface thickness used in simulation.

c_{CO2}	Spatial step	d/d_{phys}	v (cm/s)
0.08	Δx	1	634$\pm$2
	2Δx	1	757$\pm$2
0.07	Δx	1	317$\pm$2
	Δx	2	357$\pm$3
	2Δx	2	336$\pm$4
0.06	Δx	1	156$\pm$2
	Δx	2	166$\pm$3
	2Δx	2	159$\pm$3
0.05	Δx	1	75.2$\pm$3
	Δx	2	80.8$\pm$4
	2Δx	2	76.2$\pm$4

mole fractions of $c=0.05$, 0.06, 0.07, and 0.08. The corresponding growth forms are shown in Fig. 7. Our computations have been performed on a rectangular grid of 4096 $\times$4096 size, with a spatial step of 0.1 nm. The steady state growth rate can be observed only in simulations of sufficiently large size that provide enough space for the transition from the initially circular seed crystal into the fully grown dendrite before self-interaction via the periodic boundary condition takes place. It appears that the size we have chosen is just enough to reach a steady dendritic growth. The infinite time limit of the growth rate has been determined by linearly extrapolating the v vs $1/t$ plot, as shown in Fig. 8. The corresponding data are presented in Table II.

In order to explore the possibility of extending the computations to larger domains and later times, we have investigated the dependence of the growth rate and morphology on the interface thickness. Although doubling of the interface thickness influences the growth rate and morphology only marginally (see Figs. 8 and 9), a further increase of the interface thickness significantly increases the growth rate. We find that the composition of the hydrate phase changes only negligibly with the interface thickness. It is thus possible to accelerate the numerical studies by doubling the interface thickness and the spatial step. This enables us to model later stage growth morphologies forming after the critical time $t^*=9D_l/v^2$, corresponding to the transition to a steady state growth.[26(a)] Such simulations are shown in Fig. 10.

Plotting log v vs log c_L, we find a nearly linear relationship (Fig. 11), $\log(v,s/cm)=A+B\log c_L$ (where $A=7.866\pm0.176$ and $B=4.610\pm0.146$) that can be extrapo-

time consuming under the conditions of the experiments of Tohidi et al.,[2] we performed the simulations of dendritic solidification at increased supersaturations, well over the saturation concentration $c=0.033$, and extrapolated them to the saturation limit. We performed the calculations for the CO$_2$

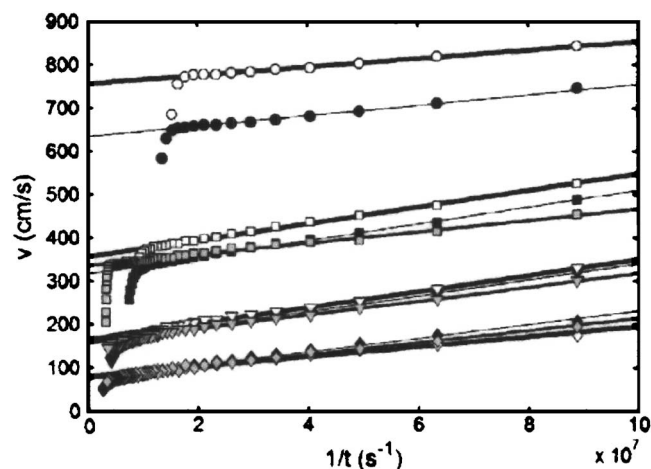

FIG. 8. Long-time extrapolation of the growth rate at different compositions, interface thicknesses, and spatial steps at $T=274.3$, K and $p=6.2$ MPa. Circles, squares, triangles, and diamonds denote the mole fraction of CO$_2$ $c=0.08$, 0.07, 0.06, and 0.05, respectively. [Black symbols stand for calculations with the physical interface thickness and the usual spatial step Δx; empty symbols denote computations performed with the doubled interface thickness and Δx; while gray-filled symbols indicate calculations with the doubled interface thickness and doubled spatial steps ($2\Delta x$).] Note the reduced growth rate at long times, where the self-interaction due to the periodic boundary condition becomes significant.
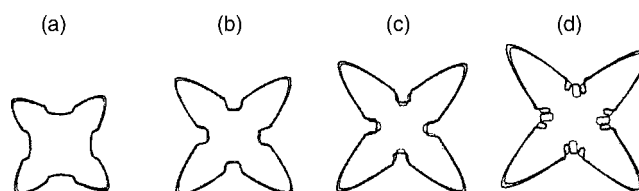

FIG. 9. Comparison of contour lines of dendrites at equal times grown with the physical interface thickness (thin line) and its double (heavy line) for CO$_2$ concentrations of (a) $c=0.05$, (b) 0.06, (c) 0.07, and (d) 0.08.
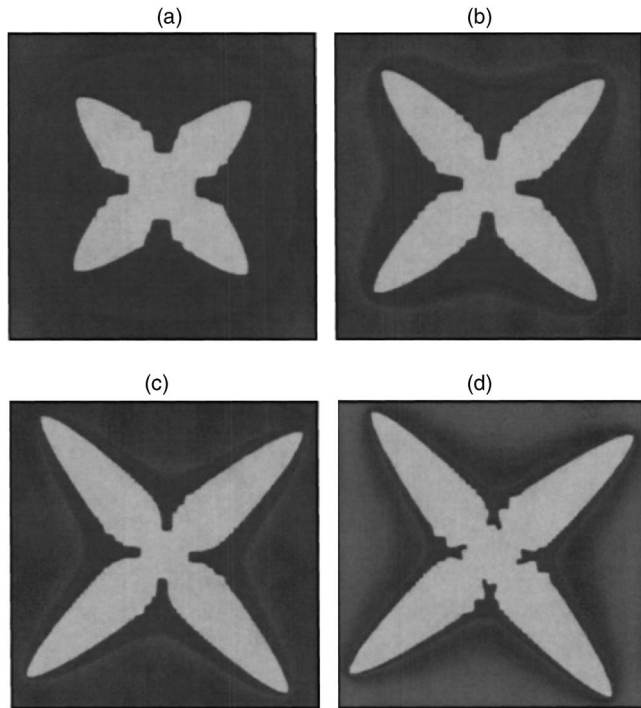
(a)   (b)

(c)   (d)

FIG. 10. CO_2 hydrate dendrites predicted on a 4096×4096 grid with a doubled spatial step (0.818×0.818 μm^2) using *twice of the physical interface thickness* in aqueous solutions of CO_2 concentrations of (a) $c=0.05$, (b) 0.06, (c) 0.07, and (d) 0.08. Snapshots of the concentration field show states reached after 1030.5, 535.5, 270, and 135 ns physical time, respectively. Note that these simulation times are larger than the critical time $t^*=9D_l/\nu^2$, after which a steady growth is expected [Ref. 26(a)].

lated to $c_L=0.033$ reasonably well (see Fig. 11). The corresponding growth rate is ~10.9 cm/s. A comparable result can be obtained from a classical treatment of the dendritic solidification based on Ivantsov's solution for the concentration field around the dendrite tip and the marginal stability criterion. A detailed comparison between the two models will be presented elsewhere.[52]

However, this value is more than three orders of magnitude higher than the experimental value (55 $\mu m/s$).[2] The
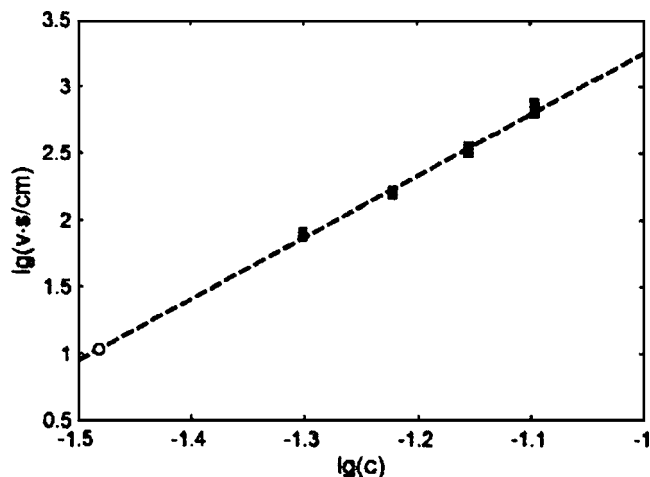

FIG. 11. Extrapolation of the composition dependent dendritic growth rate to $c_L=0.033$ (empty circle). The filled squares stand for velocities obtained from extrapolation to infinite time from Table II.

TABLE III. Sensitivity of growth velocity ν to input parameters. Reference 1: $c=0.08$, $s_0=0.065$, and $\gamma=30$ mJ/m^2. References 2 and 3: $c=0.07$, otherwise the same as reference 1. Notation: d_{phys}—physical interface thickness; d—interface thickness used in simulation.

	Spatial step	d/d_{phys}	ν (cm/s)
Reference 1	Δx	1	634 ± 2
$s_0=0.125$	Δx	1	774 ± 8
$s_0=0.05$	Δx	1	584 ± 4
$s_0=0.0375$	Δx	1	523 ± 2
$s_0=0.025$	Δx	1	449 ± 2
Reference 2	Δx	1	317 ± 2
1.1γ	Δx	1	296 ± 2
0.9γ	Δx	2	342 ± 2
Reference 3	$2\Delta x$	2	336 ± 4
With noise	$2\Delta x$	2	318 ± 6

computed growth rate and morphology might be influenced by several factors, including the sensitivity to the input data.

(i) The growth rate increases with the anisotropy of the interfacial free energy as the dendrite tip becomes more and more pointed. In the isotropic limit (diffusion controlled circular growth), for short times a continuously decreasing growth velocity $\nu \propto t^{-1/2}$ prevails, until the Mullins-Sekerka instability[53] intervenes, yielding a seaweed type growth morphology occurring also at low anisotropies.[54] However, the experiments show a faceted dendritic morphology for the CO_2 and other gas hydrate dendrites,[46] indicating a substantial (supercritical) anisotropy of either the interfacial free energy or the kinetic coefficient. This rules out the possibility that the growth rate has been overestimated in this work due to the overestimated anisotropy (see Table III).

(ii) Unlike in the case of nucleation, the experimental uncertainty of the interfacial free energy influences the growth rate only marginally (see Table III).

(iii) Fluctuations, represented by noise added to the equations of motion, are known to influence growth.[11,55] We consider the sub-molecular-size noise (of wavelength $\lambda < \lambda_0$, where the limiting wavelength $\lambda_0=0.5$ nm is about twice of the average molecular diameter) emerging from the usual unphysical treatment.[55] We introduce, therefore, a high frequency cutoff. The noise we add to the equation of motion of the phase field is obtained from a Gaussian white noise of amplitude Ξ chosen so that after removing the Fourier components of wavelength $\lambda < \lambda_0$, the final amplitude of the noise satisfies the fluctuation-dissipation relationship for the white noise on spatial scale of λ_0, $\Xi' = [2M_\phi kT/(\lambda_0^3 \Delta t)]^{1/2}$.[55] In agreement with Ref. 11, sidebranching is enhanced by the noise (Fig. 12), while the growth rate does not change significantly (see Table III).

(iv) Another (technical) possibility that cannot be ruled out entirely is that in the experiment the CO_2 content of the aqueous solution or the local temperature may deviate from the nominal values. The heterogeneous nature of the solidification structure supports this pos-
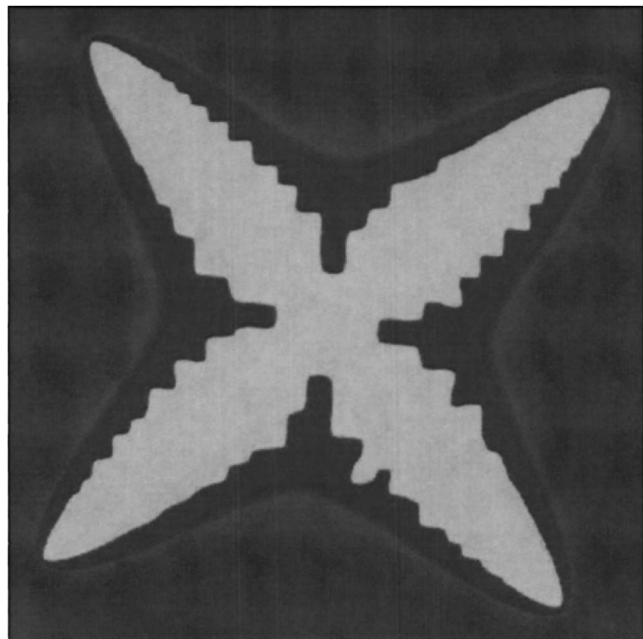
FIG. 12. CO$_2$ hydrate dendrites predicted with noise added to the phase field equation on a 4096×4096 grid with doubled spatial step (0.818×0.818 μm^2) using *twice of the physical interface thickness* in the aqueous solution of a CO$_2$ concentration of 0.07. The snapshot of the concentration field shows the state reached after 270 ns physical time. Note the enhanced side undulations relative to Figs. 7(c) and 10(c) on the sides of the primary branches that may lead to the formation of secondary arms at later stages of growth.

sibility. While the dilution of the solution certainly would reduce the driving force, and thus the growth rate, the respective inhomogeneity should be quite substantial to explain the observed three orders of magnitude difference in the growth rate, which we think has a rather low probability. We may also consider that if the equilibration of the aqueous solution happened at room temperature (20 °C) in the experiment, the mole fraction of CO$_2$ has to be somewhat lower, $c \approx 0.026$, yielding a lower velocity $\nu \approx 3.6$ cm/s, another effect far too small to account for the observed deviations.

(v)   The CO$_2$ hydrate has a remarkably complex crystal structure, thus its formation from the aqueous solution requires a complicated molecular motion at the interface and may represent a kinetic barrier against growth. It is, therefore, possible that the kinetic coefficient (and the phase field mobility) is smaller than the one for the purely translational diffusion controlled growth assumed here. Further MD studies are needed to see whether this explanation indeed applies.

Since possibilities (i)–(iii) cannot account for the observed discrepancy between experiment and theory, and a significant effect from (iv) is rather improbable, it appears that (v) is responsible for the deviations. This is supported by the fact that we experienced difficulties when trying to grow hydrate phases from an aqueous solution in MD simulations, a finding that suggests that a substantial kinetic barrier might indeed be present, hindering the growth of the hydrate phase. (Such a reduced kinetic coefficient would be entailed by a proportional reduction of the nucleation rates presented herein, further reinforcing our conclusion that the homogeneous CO$_2$ hydrate nucleation in aqueous CO$_2$ solutions can be ruled out in general.) We note finally that computations of hydrate dendrites with orders of magnitude smaller phase field mobilities are beyond the abilities of the numerical model used in this paper. This problem may be addressed (without noise) using the adaptive grid technique of Provatas *et al.*[26(a)] The treatment of Vetsigian and Goldenfeld[56] to kinetics controlled growth might be another suitable approach. Work is underway to investigate these possibilities.

V. SUMMARY

We have applied a multiscale approach based on phase field modeling with parameters deduced from experiment and molecular dynamics simulation to calculate the nucleation and growth rates of CO$_2$ hydrate in aqueous solutions under conditions typical to seabed reservoirs. We find that, on the human time scales, a homogeneous nucleation can be ruled out as a possible mechanism for initiating a hydrate formation. Furthermore, the growth rates predicted by theory are about three orders of magnitude too high. While several possibilities have been investigated, a kinetic barrier against hydrate growth due to the complex molecular motions required for crystal growth appears to be the most probable source of discrepancy.

ACKNOWLEDGMENTS

[1] L. Milich, Global Environ. Change **9**, 179 (1999); K. A. Kwenvolden, Proc. Natl. Acad. Sci. U.S.A. **96**, 3420 (1999); E. D. Sloan, Jr., Nature (London) **426**, 353 (2003).

[2] B. Tohidi, R. Anderson, M. B. Clenell, R. W. Burgass, and A. B. Biderkab, Geology **29**, 867 (2001).

[3] Recent review on gas hydrate research: *Advances in the Study of Gas Hydrates*, edited by C. E. Taylor and J. T. Kwan (Springer, Berlin, 2004).

[4] B. Kvamme, A. Graue, E. Aspenes, T. Kuznetsova, L. Gránásy, G. Tóth, and T. Pusztai, Phys. Chem. Chem. Phys. **6**, 2327 (2004).

[5] L. Gránásy, T. Pusztai, G. Tegze, T. Kuznetsova, and B. Kvamme, *Advances in the Study of Gas Hydrates* (Ref. 3), Chap. 1.

[6] Recent reviews on the phase field approach: (a) W. J. Boettinger, J. A. Warren, C. Beckermann, and A. Karma, Annu. Rev. Mater. Res. **32**, 163 (2002); (b) L. Q. Chen, *ibid.* **32**, 113 (2002); (c) J. J. Hoyt, M. Asta, and A. Karma, Mater. Sci. Eng., R. **41**, 121 (2003); (d) L. Gránásy, T. Pusztai, and J. A. Warren, J. Phys.: Condens. Matter **16**, R1205 (2004).

[7] (a) L. Gránásy, J. Mol. Struct. **485/486**, 523 (1999); (b) L. Gránásy and T. Pusztai, J. Chem. Phys. **117**, 10121 (2002); (c) L. Gránásy, T. Börzsönyi, and T. Pusztai, Phys. Rev. Lett. **88**, 206105 (2002); (d) J. Cryst. Growth **237–239**, 1813 (2002); (e) M. Castro, Phys. Rev. B **67**, 035412 (2003); (f) L. Gránásy, T. Pusztai, G. Tóth, Z. Jurek, M. Conti, and B. Kvamme, J. Chem. Phys. **119**, 10376 (2003).

[8] R. Kobayashi, J. A. Warren, and W. C. Carter, Physica D **119**, 415 (1998); B. Nestler and A. A. Wheeler, *ibid.* **138**, 114 (2000); B. Nestler, A. A. Wheeler, L. Ratke, and C. Stocker, *ibid.* **141**, 133 (2000); M. Plapp and A. Karma, Phys. Rev. E **66**, 061608 (2002); L. Gránásy, T. Pusztai, J. A. Warren, J. F. Douglas, T. Börzsönyi, and V. Ferreiro, Nat. Mater. **2**, 92 (2003); L. Gránásy, T. Pusztai, T. Börzsönyi, J. A. Warren, and J. F. Douglas, *ibid.* **3**, 645 (2004); D. Danilov and B. Nestler, Phys. Rev. Lett.

93, 215501 (2004); L. Gránásy, T. Pusztai, G. Tegze, J. A. Warren, and J. F. Douglas, Phys. Rev. E **72**, 011605 (2005).

[9] If the volume integral of a field is constant throughout the time evolution of the system, it is called a conserved field, while the volume integral of nonconserved fields changes with time.

[10] Y. C. Shen and D. W. Oxtoby, J. Chem. Phys. **105**, 6517 (1996).

[11] J. A. Warren and W. J. Boettinger, Acta Metall. Mater. **43**, 689 (1995).

[12] J. M. Howe, Philos. Mag. A **74**, 761 (1996); W. J. Huisman, J. F. Peters, M. J. Zwanenburg, S. A. de Vries, T. E. Derry, D. Abernathy, and J. F. van der Veen, Nature (London) **390**, 379 (1997).

[13] For example, J. Q. Broughton, G. H. Gilmer, and K. A. Jackson, Phys. Rev. Lett. **49**, 1496 (1982); B. B. Laird and A. D. J. Haymet, Chem. Rev. (Washington, D.C.) **92**, 1819 (1992); R. L. Davidchack and B. B. Laird, J. Chem. Phys. **108**, 9452 (1998).

[14] S. L. Wang, R. F. Sekerka, A. A. Wheeler, B. T. Murray, S. R. Coriell, R. J. Braun, and G. B. McFadden, Physica D **69**, 189 (1993).

[15] Strictly, this widely used formulation of the anisotropy is appropriate for modeling 2D or quasi-two-dimensional systems, where the orientation field is simply a scalar. Therefore, it is suitable for, e.g., the description of transformations in thin layers of thickness L, where along thickness (direction z) the system is considered uniform. A true three-dimensional (3D) free energy functional would depend on a 3D orientation field and 3D unit vectors defining the orientation of the surface normal as described in, e.g., T. Pusztai, G. Bortel, and L. Gránásy, Europhys. Lett. **71**, 131 (2005); R. Kobayashi and J. Warren, Physica A **356**, 127 (2005).

[16] J. W. Cahn and J. E. Hilliard, J. Chem. Phys. **28**, 258 (1958).

[17] Atomistic simulations: W. C. Swope and H. C. Andersen, Phys. Rev. B **41**, 7024 (1990); L. A. Báez and P. Clancy, J. Chem. Phys. **102**, 8138 (1995); P. R. ten Wolde, M. J. Ruiz-Montero, and D. Frenkel, Phys. Rev. Lett. **75**, 2714 (1995); S. Auer and D. Frenkel, Nature (London) **409**, 1020 (2001); **413**, 711 (2001). Experiment: U. Gasser, E. R. Weeks, A. Schofield, P. N. Pusey, and D. A. Weitz, Science **292**, 258 (2001).

[18] J. W. Cahn and J. E. Hilliard, J. Chem. Phys. **31**, 688 (1959).

[19] D. W. Oxtoby, *Liquids, Freezing and Glass Transition*, edited by J. P. Hansen, D. Levesque, and J. Zinn-Justin (Elsevier, Amsterdam, 1991), p. 145; Annu. Rev. Mater. Res. **32**, 39 (2002).

[20] K. F. Kelton, Solid State Phys. **45**, 75 (1991).

[21] K. F. Kelton and A. L. Greer, Phys. Rev. B **38**, 10089 (1988); A. L. Greer and K. F. Kelton, J. Am. Ceram. Soc. **75**, 1015 (1991).

[22] A. Masuhr, T. A. Waniuk, R. Busch, and W. L. Johnson, Phys. Rev. Lett. **82**, 2290 (1999); K. L. Ngai, J. H. Magill, and D. J. Plazek, J. Chem. Phys. **112**, 1887 (2000); S. F. Swallen, P. A. Bonvallet, R. J. McMahon, and M. D. Ediger, Phys. Rev. Lett. **90**, 015901 (2003).

[23] M. Conti, Phys. Rev. E **56**, 3197 (1997).

[24] (a) A. Karma and W. J. Rappel, Phys. Rev. E **53**, R3017 (1996); (b) **57**, 4323 (1998); (c) A. Karma, Phys. Rev. Lett. **87**, 115701 (2001); (d) B. Etchebarria, R. Folch, A. Karma, and M. Plapp, Phys. Rev. E **70**, 061604 (2004).

[25] J. Bragard, A. Karma, Y. H. Lee, and M. Plapp, Interface Sci. **10**, 121 (2002); R. Folch and M. Plapp, Phys. Rev. E **68**, 010602 (2003).

[26] (a) N. Provatas, N. Goldenfeld, and J. Dantzig, Phys. Rev. Lett. **80**, 3308 (1998); (b) R. Tonhardt and G. Amberg, J. Cryst. Growth **194**, 406 (1998); (c) M. Sabouri-Ghomi, N. Provatas, and M. Grant, Phys. Rev. Lett. **86**, 5084 (2001); (d) J. C. Ramirez and C. Beckermann, Trans. Ind. Inst. Matels **58**, 523 (2005).

[27] (a) R. L. Davidchack and B. B. Laird, Phys. Rev. Lett. **85**, 4751 (2000); (b) J. J. Hoyt, M. Asta, and A. Karma, *ibid.* **86**, 5530 (2002); (c) J. J. Hoyt and A. Karma, Phys. Rev. B **65**, 214106 (2002); (d) M. Asta, J. J. Hoyt, and A. Karma, *ibid.* **66**, 100101 (2002); (e) J. R. Morris, *ibid.* **66**, 144104 (2002); (f) J. R. Morris, Z. Y. Lu, Y. Y. Ye, and K. M. Ho, Interface Sci. **10**, 143 (2002); (g) J. R. Morris and X. Song, J. Chem. Phys. **119**, 3920 (2003); (h) B. Laird and R. Davidchack, Biometrika **109**, 17802 (2005); (i) R. L. Davidchack, J. R. Morris, and B. B. Laird, J. Phys. Chem. B **109**, 6500 (2005).

[28] M. Frigo and S. G. Johnson, Proc. IEEE **93**, 216 (2005).

[29] M. von Stackelberg and H. R. Müller, Z. Elektrochem. **58**, 25 (1954).

[30] M. von Stackelberg and W. Jahns, Z. Elektrochem. **58**, 162 (1954).

[31] H. J. C. Berendsen, J. P. M. Postma, W. F. van Gunsterer, and J. Hermans, *Intermolecular Forces*, edited by B. Pullman (Reidel, Dordrecht, 1981).

[32] J. G. Harris and K. H. Yung, J. Phys. Chem. **99**, 12021 (1995).

[33] A. P. Lyubartsev and A. Laaksonen, Comput. Phys. Commun. **128**, 565 (2000).

[34] G. J. Martyna, D. J. Tobias, and M. L. Klein, J. Chem. Phys. **101**, 4177 (1994).

[35] S. Nosé, Prog. Theor. Phys. Suppl. **103**, 1 (1991).

[36] W. G. Hoover, Phys. Rev. A **31**, 1695 (1985).

[37] D. Fincham, Mol. Simul. **8**, 165 (1992).

[38] T. Bryk and A. D. J. Haymet, J. Chem. Phys. **117**, 10258 (2002).

[39] B. Kvamme and H. Tanaka, J. Phys. Chem. **99**, 7114 (1995).

[40] L. W. Diamond and N. N. Akinfiev, Fluid Phase Equilib. **208**, 265 (2003).

[41] A. Svandal and B. Kvamme, Phys. Chem. Chem. Phys. **8**, 1707 (2006).

[42] H. Teng and A. Yamasaki, J. Chem. Eng. Data **43**, 2 (1998).

[43] R. Anderson, M. Llamedo, B. Tohidi, and R. W. Burgass, J. Phys. Chem. B **107**, 3507 (2003).

[44] S. C. Hardy, Philos. Mag. **35**, 471 (1977).

[45] D. Kashchiev and A. Firoozabadi, J. Cryst. Growth **243**, 476 (2002).

[46] T. Uchida, T. Ebinuma, J. Kawabata, and H. Narita, J. Cryst. Growth **204**, 348 (1999); Z. Huo, K. Hester, E. D. Sloan, Jr., and K. T. Miller, AIChE J. **49**, 1300 (2003).

[47] J. J. Eggleston, G. B. McFadden, and P. W. Voorhees, Physica D **150**, 91 (2001); J. M. Debierre, A. Karma, F. Celestini, and R. Guerin, Phys. Rev. E **68**, 041604 (2003).

[48] M. Panhuis, C. H. Patterson, and R. M. Lynden-Bell, Mol. Phys. **94**, 963 (1988).

[49] D. Turnbull, J. Appl. Phys. **21**, 1022 (1950); J. Chem. Phys. **18**, 768 (1950).

[50] R. M. Pratt and E. D. Sloan, Mol. Simul. **15**, 247 (1995); R. M. Pratt, D.-H. Mei, T.-M. Guo, and E. D. Sloan, J. Chem. Phys. **106**, 4187 (1997).

[51] Various theoretical studies indicate that the induction time of nucleation θ is proportional to $1/D$, where D is the self-diffusion coefficient in the liquid phase [see, e.g., K. F. Kelton, A. L. Greer, and C. V. Thompson, J. Chem. Phys. **79**, 6261 (1983), henceforth referenced as KGT]. Here, we use the expression by Kashchiev [see Eq. (31) of KGT] to estimate the induction time, while for a lithium-disilicate glass of viscosity of ~4.5 $\times 10^9$ Pa s at 750 K, one obtains an induction time of $\theta = 62.6$ s (KGT). In our reference aqueous solution, the induction time after which the steady state nucleation (of extremely low rate) is established is only $\theta = 0.33$ ns. This ~11 orders of magnitude difference in the induction time originates mainly from an almost 14 orders of magnitude difference in the self-diffusion coefficient.

[52] L. Gránásy, T. Pusztai, and G. Tegze (unpublished).

[53] W. W. Mullins and R. F. Sekerka, J. Appl. Phys. **34**, 323 (1963); **35**, 444 (1964).

[54] For example, T. Ihle and H. Müller-Krumbhaar, Phys. Rev. E **49**, 2972 (1994); E. Brener, H. Müller-Krumbhaar, D. Temkin, and T. Abel, Physica A **249**, 73 (1998).

[55] A. Karma and W.-J. Rappel, Phys. Rev. E **60**, 3614 (1998).

[56] K. Vetsigian and N. Goldenfeld, Phys. Rev. E **68**, 060601 (2003).